Contributed paper

OPTO-ELECTRONICS REVIEW **11**(4), 305–311 (2003)

Application of polarisation-maintaining side-hole fibres to direct force measurement

P. WIERZBA* and B.B. KOSMOWSKI

Gdansk University of Technology, Department of Optoelectronics,
11 Narutowicza Str., 80-952 Gdańsk, Poland

The use of single mode polarization-maintaining side-hole (SMPM-SH) fibres for direct measurement of transverse force has been studied theoretically and experimentally. Based on the results of a qualitative analysis of stress distribution in such a fibre, it was predicted that SMPM-SH fibres can exhibit higher sensitivity to transverse force than a standard SMPM fibre. The modelling of two types of SMPM-SH fibres with bow-tie and round holes was conducted using finite element method and modified coupled-mode method. It showed that while there is a marked increase of the sensitivity for the SMPM-SH fibre with bow-tie holes, the sensitivity of the SMPM-SH fibre with round holes can be even lower than that of a standard SMPM fibre. Subsequently, in an experiment, which to the authors' knowledge is the first application of SMPM-SH fibres to direct transverse force measurement, the sensitivity of an SMPM-SH fibre with bow-tie holes was measured. Measurement results agreed well with theoretical predictions. However, more systematic research is needed to determine the relationship between the sensitivity, dimensions and geometry of the holes.

Keywords: force measurement, fibre sensor, polarisation, optical fibre, birefringence, finite element modelling, side-hole fibre.

1. Introduction

Single mode polarization-maintaining side-hole (SMPM--SH) fibres have been developed mainly for applications in polarimetric pressure sensors. By modifying a standard SMPM fibre, shown in Fig. 1(a), by the introduction of holes filled with air in the cladding, as shown in Fig. 1(b), stress distribution in the core region is altered and pressure sensitivity at SMPM-SH fibres can be increased, compared to that of a standard SMPM fibre. The increase is substantial - up to two orders of magnitude [1].

Similarly, sensitivity of an SMPM fibre to transverse force acting along the *y* axis [c.f. Fig. 1(c)], depends also on stress distribution in the core region in the manner discussed in the following Section. By introducing side holes, as shown in Fig. 1(d), stress distribution in the core region is altered. From qualitative analysis, outlined in the following Section, it follows that SMPM-SH fibres can exhibit higher sensitivity to transverse force than standard SMPM fibres.

To verify this hypothesis selected types of SMPM-SH fibres were modelled using coupled mode theory outlined in Section 2 and finite element method. Results of modelling are discussed in Section 3. Finally, the experiment described in Section 4 was performed using available SMPM-SH fibres to provide a proof of the hypothesis. Conclusions and scope of future research is given in Section 5.

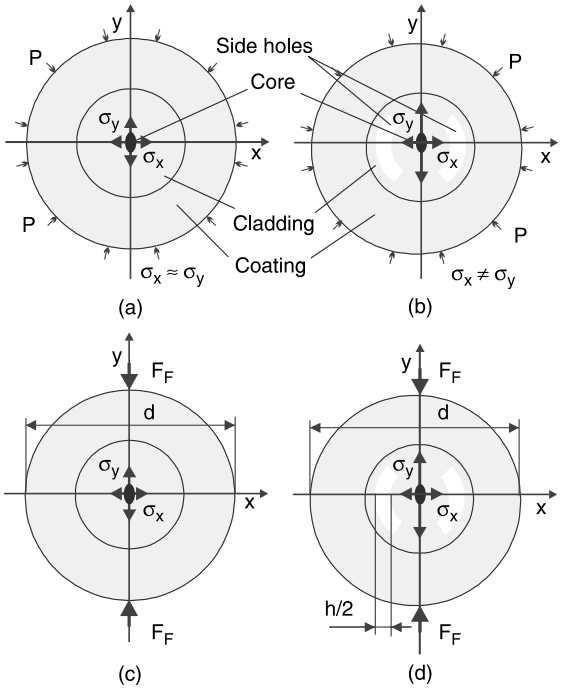

Fig. 1. Single mode polarization maintaining fibres, (a) standard SMPM fibre subjected to hydrostatic pressure, (b) SMPM-SH fibre subjected to hydrostatic pressure, (c) standard SMPM fibre subjected to transverse force, (d) SMPM-SH fibre subjected to transverse force. P is the hydrostatic pressure, F_F is the transverse force, σ_x, σ_y are the stress components in fibre's core centre, d is the diameter of the fibre, $h/2$ is the width of the side hole, and z is the axis direction is out of the page.

*e-mail: opto@eti.pg.gda.pl

2. Theory

Polarimetric pressure and transverse force sensors discussed in this paper respond to the measurand with change of phase difference between two polarization modes HE_{11}^{x} and HE_{11}^{y} propagating in an SMPM fibre. Calculation of their response as a function of pressure or force acting on a segment of sensing fibre is conducted in two steps. First, stress components (σ_x, σ_y, τ_{xy}) in the core region of the sensing fibre are calculated (typically using finite element method) assuming plane strain state in the sensing fibre [2]). Second, modified coupled-mode method is used to calculate phase change of polarization modes in perturbed fibre, based on stress components calculated in the previous step.

Elliptic core SMPM and SMPM-SH fibres analysed in the remainder of this paper have cross-sections symmetrical about x and y axes, as those of fibres shown in Fig. 1, and are made from materials that are isotropic, homogeneous and follow Hooke's law. In such fibres, subjected to the hydrostatic pressure P or to the transverse force F acting along x or y axis, stress distribution is also symmetrical about x and y axes. It follows from this that principal directions of stress [2] in the origin of the coordinate system $0xy$ (i.e., in the core centre) are parallel to the axes of the coordinate system and that $\tau_{xy} = 0$.

The electric field vector E of electromagnetic wave propagating in a fibre subjected to perturbation can be expressed, according to modified coupled-mode theory [3,4], as a linear combination of the electric field vectors e_x, e_y of the polarization modes in the unperturbed fibre

$$E = \left(A(z)e_x + B(z)e_y\right)\exp(j\omega t), \tag{1}$$

where $A(z)$, $B(z)$ are the electric field amplitudes, and ω is the angular frequency of the light.

The electric field amplitudes $A(z)$ and $B(z)$ depend only on the fibre axis coordinate z. They also have to satisfy coupled mode equations [3]

$$\frac{d}{d_z}\begin{bmatrix} A \\ B \end{bmatrix} = -j\begin{bmatrix} N_{11} & N_{12} \\ N_{21} & N_{22} \end{bmatrix}\cdot\begin{bmatrix} A \\ B \end{bmatrix}, \tag{2}$$

where N_{ij} are the coupling coefficients, whose values depend upon perturbations acting on the fibre in the manner discussed in Ref. 3. Solution of Eq. (2) for arbitrary initial amplitudes A_0 and B_0 exists and has the form

$$\begin{aligned} A(z) &= A_0\exp(-j\beta_1 z), \\ B(z) &= B_0\exp(-j\beta_2 z) \end{aligned} \tag{3}$$

where β_1, β_2 are the propagation constants of the polarization modes HE_{11}^{x} and HE_{11}^{y}.

By substituting Eq. (3) into Eq. (2) and solving the resulting equations, the propagation constants β_1, β_2 can be expressed in terms of coupling coefficients N_{ij}. Their difference $\Delta\beta = |\beta_1 - \beta_2|$ takes the form [3]

$$\Delta\beta = \sqrt{(N_{11} - N_{22})^2 + |2N_{12}|^2}. \tag{4}$$

Assuming that the average stress in the core region can be approximated by the stress in the core centre, and taking into account fact that $\tau_{xy} = 0$, the coupling coefficients N_{ij} can be expressed as [5]

$$\begin{aligned} N_{11} - N_{22} &= \frac{2\pi}{\lambda}\left[B + C(\sigma_y - \sigma_x)\right], \\ N_{12} &= N_{21} = 0 \end{aligned} \tag{5}$$

where B is the intrinsic birefringence of the fibre (stress-induced or caused by an elliptic core), C is the elastooptic coefficient of fibre core material, σ_x, σ_y are the stress components in fibre's core centre, in direction x and y, respectively, and λ is the free-space wavelength of the light propagating in the fibre.

Substitution for coupling coefficients N_{ij} from Eq. (5) into Eq. (4) gives

$$\Delta\beta = \frac{2\pi}{\lambda}\left|B + C(\sigma_y - \sigma_x)\right|. \tag{6}$$

It should be noted that neither the pressure P nor the force F appear in Eq. (6) in an explicit form. This stems from the fact that the relation between P or F and stress components σ_x, σ_y depends on dimensions of the fibre, shape and dimensions of side holes for SMPM-SH fibres and on elastic properties of materials from which the fibre is made. For a standard SMPM fibre, σ_x and σ_y can be found from theory of elasticity [2] whereas for SMPM-SH fibres they have to be calculated numerically, for example, using finite element method.

The phase difference $\Delta\varphi$ of the polarization modes arising due to the action of the transverse force F_p evenly distributed along the sensing fibre segment of the length l can be calculated from the formula

$$\Delta\varphi = (\Delta\beta_F - \Delta\beta_0)l = \left(\frac{2\pi}{\lambda}\left|B + C(\sigma_y - \sigma_x)\right| - \frac{2\pi}{\lambda}|B|\right)l, \tag{7}$$

where $\Delta\beta_F$ is the difference of propagation constants of polarization modes when the force F_p is acting on the fibre segment, $\Delta\beta_0$ is the difference of propagation constants of polarization modes in the unperturbed fibre segment, B is the birefringence of the fibre (stress-induced or caused by an elliptic core), C is the elastooptic coefficient of fibre core material, σ_x, σ_y are the stress components in fibre's core centre, in direction x and y, respectively, λ is the free-space wavelength of the light propa-

gating in the fibre, and l is the length of the fibre segment on which force F_p is acting.

For most SMPM fibres their intrinsic birefringence B is higher than $C(\sigma_x - \sigma_y)$. Therefore, $\Delta\beta_F$ does not change sign as a result of force acting on the fibre, Eq. (7) becomes

$$\Delta\varphi = \frac{2\pi}{\lambda}\left|C(\sigma_y - \sigma_x)\right|l. \tag{8}$$

The same formula holds for hydrostatic pressure acting on the fibre. By using that to express sensitivity K_P of the fibre to hydrostatic pressure, defined as in Ref. 6, one arrives at

$$K_P = \frac{\Delta\varphi}{Pl} = \frac{2\pi|C|}{\lambda}\frac{\left|\sigma_y - \sigma_x\right|}{P}, \tag{9}$$

where $\Delta\varphi$ is the phase difference of polarization modes induced by the hydrostatic pressure, l is the length of the fibre, P is the hydrostatic pressure acting on a fibre.

Finally, to facilitate the comparison of results obtained for different fibres, it is possible to define sensitivity of the fibre to the transverse force K_F as

$$K_F = \frac{\Delta\varphi}{F_p} = \frac{2\pi l|C|}{\lambda}\frac{\left|\sigma_y - \sigma_x\right|}{F_p}, \tag{10}$$

where $\Delta\varphi$ is the phase difference of polarization modes induced by force acting on fibre and F_p is the transverse force.

The SMPM fibre from Fig. 1(a) shows almost perfect central symmetry (elliptical core has mechanical properties very similar to those of the cladding, as indicated in Table 1). If hydrostatic pressure is acting on the fibre, as shown in Fig. 1(a), stress state has also almost perfect central symmetry. As a result $\sigma_x \approx \sigma_y$, and from Eq. (9) it follows immediately that this fibre has K_P close to zero. If a fibre does not have a central symmetry, as the SMPM-SH fibre from Fig. 1(b), then a stress state resulting from the action of hydrostatic pressure does not have circular symmetry as well. In such a fibre, stress components are not equal, i.e. ($\sigma_x \neq \sigma_y$), and its sensitivity K_P to a hydrostatic pressure is much higher than that of the SMPM fibre.

For fibres subjected to a transverse force it follows from Eq. (10) that in order to increase K_F without changing operating wavelength λ or altering core material (i.e., C = const.) one has to increase $|\sigma_y - \sigma_x|/F_p$ (it should be noted here that no increase of K_F by increasing l is possible. If the length l of the fibre is increased, the force F_p becomes distributed over a longer length of fibre which results in a decrease of the stress components σ_x and σ_y, proportional to the increase of l, keeping K_F constant. This can be accomplished by introduction of side holes in the fibre's cladding and can be explained as follows. In the length l of an SMPM fibre of the diameter d [c.f. Fig. 1(c)], subjected to the transverse force F_p, the average stress component σ_{yAVR}, which is the ratio of force to the area of the fibre's cross-section by the plane $0xz$, is equal to

$$\sigma_{yAVR} = \frac{F_p}{ld}. \tag{11}$$

By introducing side holes [c.f. Fig. 1(d)] area of the fibre's cross-section by the plane $0xz$ is decreased, and σ_{yAVR} is now equal

$$\sigma_{yAVR} = \frac{F_p}{l(d-h)} \tag{12}$$

and it is higher than for SMPM fibre. Therefore, it is reasonable to expect an increase of σ_y in the core centre. If this increase is not accompanied by an increase of σ_x by at least the same amount, sensitivity K_F also increases, according to (10).

Table 1. Young modulus and Poisson's ratio of fibre's materials.

	Young modulus E (Gpa)	Poisson's ratio v
Silica glass (cladding)	72.45	0.17
Silica glass (core)	72.37	0.1698
Coating	1.035	0.35

3. Modelling

Primary objective of modelling was determination of sensitivity K_F of example fibres to transverse force. A commercial finite element analysis (FEA) package ANSYS was used to calculate stress components σ_x, σ_y in the cores of the fibres. Based on calculated values of σ_x and σ_y, K_F was calculated from Eq. (10). Three types of fibres were modelled: a standard SMPM fibre shown in Fig. 2(a), an SMPM-SH Bow-Tie fibre shown in Fig. 2(b), and an SMPM-SH Radial Hole fibre shown in Fig. 2(c). In further discussion the latter two fibres will be referred to as the BT fibre and the RH fibre, respectively, whereas the first fibre will be referred to as the standard fibre. The standard fibre was modelled for reference purposes to detect numerical problems which can occur during FEA calculations. All fibres have a cladding diameter 125 μm and a coating diameter 250 μm. Their coating is composed from one layer of hard varnish which is typically used for the outer layer of telecommunication fibres' coating. Moreover, it is assumed that all fibre materials, whose elastic properties are shown in Table 1, are homogeneous, isotropic and follow Hooke's law.

As a reference, calculation of stress components for the standard fibre has been carried out. Based on its results K_F

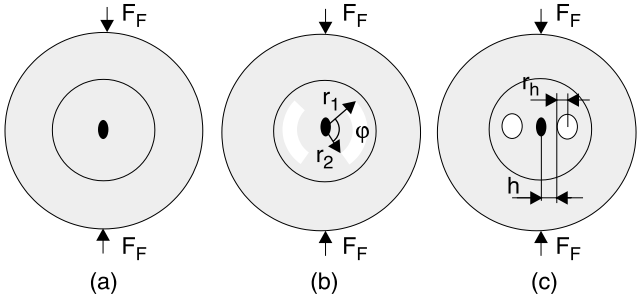

Fig. 2. Cross-sections of modelled SMPM fibres: (a) standard fibre, (b) SMPM-SH BT fibre, (c) SMPM-SH RH fibre, r_1 is the outer radius, r_2 is the inner radius, φ is the central angle, h is the distance from the core centre to the hole perimeter, and r_h is the radius of side hole.

was found to be 0.4136 rad/N, which agrees well with measured value of 0.41 rad/N reported in Ref. 7 for a fibre having the same dimensions and made of the same materials.

Following, stress components were calculated for the BT fibre presented in Fig. 2(b). Side hole shape was assumed to be a circular ring segment having the central angle $\varphi = 135°$. During the analysis inner and outer radii (r_1 and r_2, respectively) of the circular ring segment were varied. The sensitivity K_F for different values of these radii is shown in Table 2, along with the sensitivity K_{FN} is normalized to that of the standard fibre, i.e.

$$K_{FN} = \frac{K_F}{K_{FS}}, \tag{13}$$

where K_F is the sensitivity of the analysed fibre to transverse force, K_{FS} is the sensitivity of the standard fibre to transverse force, K_{FN} is the normalized sensitivity of the analysed fibre to transverse force.

It can be seen from Table 2 that the sensitivity K_F of the BT fibre increases with increasing the outer radius r_1, and decreases with increasing r_2. Moreover, the sensitivity K_F of this fibre is always greater than that of the reference fibre, and over fourfold increase in sensitivity, compared to the reference fibre, is possible.

Finally, the sensitivity K_F of the RH fibre, Fig. 2(c), was calculated. During the analysis the hole radius r_h and distance from core centre to the hole perimeter h were varied. Initial modelling results provided no clear relationship between K_F and the two parameters. Moreover, for some parameter values the sensitivity K_F was lower than that of reference fibre.

In order to prove that this unexpected result was not caused by an error in the model or by numerical problem, an independent verification was carried out using another commercial finite element analysis program (COSMOS) and by estimating stress components using theory of elasticity. In both cases, the obtained results confirmed our previous findings. Detailed examination of stress values in the fibre shown that the phenomenon responsible for such behaviour is stress concentration on the border of holes in the area surrounding the fibre's core [2]. When the distance from the core centre to the hole perimeter h is decreased, the stress component σ_y in the core centre decreases faster than σ_x, as it can be seen in Fig. 3. As a result, $|\sigma_y - \sigma_x|$ decreases, which in turn results in a decrease in the sensitivity K_F because of Eq. (10).

Table 2. Sensitivity K_F to transverse force and normalized sensitivity K_{FN} of the BT fibre for different fibre geometries.

Outer radius r_1 (μm)	Inner radius r_2 (μm)	Sensitivity K_F (rad/N)	Normalised sensitivity K_{FN}
30	15	0.8848	2.14
40	15	1.3151	3.18
50	15	1.7692	4.28
30	20	0.7136	1.73
40	20	1.0246	2.48
50	20	1.3441	3.25

In order to provide a better insight into dependence of the sensitivity K_F from r_h and h, the range of h was extended down to $h_{min} = 5$ μm, i.e., beyond a limit imposed by the mode field diameter of light propagating in the fibre. Resulting values of K_F are shown in Table 3, and the sensitivity K_{FN} normalized to that of the standard fibre is presented in Table 4 and in Fig. 4.

Based on the data from Table 4 and Fig. 4 it is possible to note that for the larger hole radii r_h (15 μm and 20 μm) the sensitivity K_{FN} increases when the distance between the core and the holes decreases. Similarly, for $h = 5$ μm, K_{FN}

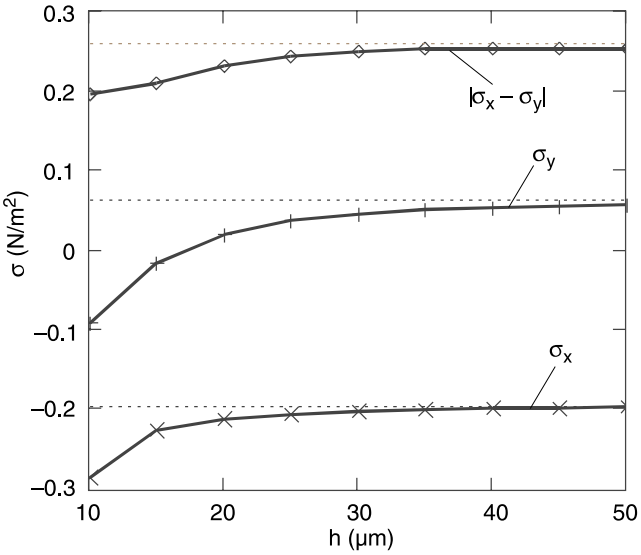

Fig. 3. Stress components in the RH fibre as a function of distance from the core centre to the hole perimeter h for radius of side hole $r_h = 5$ mm. –x– σ_x –+– σ_y, –◆– $|\sigma_y - \sigma_x|$. Dotted asymptotes mark values of respective stress components for the standard fibre.

Table 3. Sensitivity to transverse force K_F of RH fibre for different fibre geometries. ◆– side hole would extend beyond cladding for this h and r_h.

Sensitivity K_F (rad/N)		Distance from core centre to hole perimeter h (μm)								
		5	10	15	20	25	30	35	40	45
Hole radius r_h (μm)	5	0.311	0.334	0.369	0.388	0.398	0.403	0.405	0.405	0.405
	10	0.522	0.334	0.343	0.359	0.370	0.374	0373	◆	◆
	15	0.858	0.450	0.364	0.344	0.334	◆	◆	◆	◆
	20	1.286	0.624	0.424	◆	◆	◆	◆	◆	◆

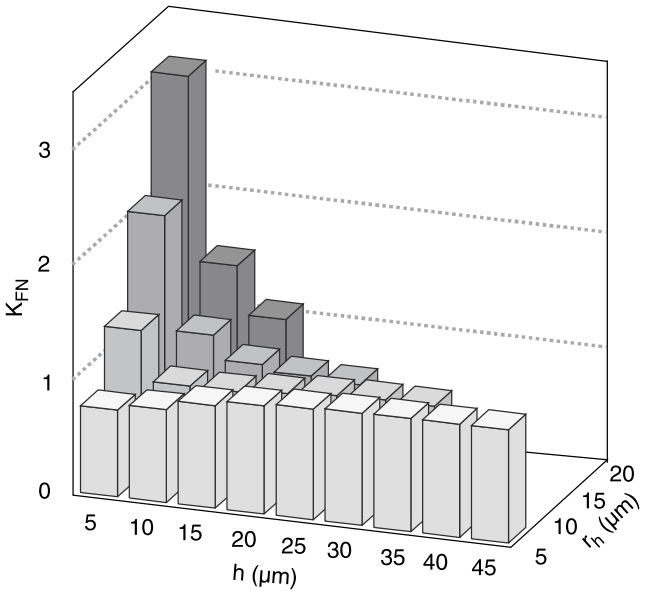

Fig. 4. Normalised sensitivity K_{FN} of the RH fibre as a function of distance from the core centre to the hole perimeter h and radius of the side hole r_h.

increases with increasing hole radius. If the hole radius r_h is 5 μm or 10 μm, then a 18–23% decrease in K_{FN} is observed as h is decreased. For h = 10 μm, this is followed by a sharp increase in K_{FN} up to 1.26. Moreover, it should be noted that for almost all values of r_h and h for which an RH fibre has loss acceptable in sensing applications (i.e., less than 100 dB/km at 633 nm), its sensitivity K_F is lower than that of the standard fibre.

4. Experiment

To verify the results obtained using finite element analysis, sensitivity to transverse force of three SMPM-SH fibres was measured. The fibres, produced at the Univeristy of Maria Curie-Skłodowska, were designed for single mode operation at 633 nm, had 125 μm cladding diameter and were coated in hard varnish (coating diameter 250 μm). Their mechanical parameters are presented in Table 1. The first fibre was a standard elliptical core SMPM fibre, whereas two latter ones were SMPM-SH fibres from production lots 960613 XI and 960308 VI. Sensitivity to the hydrostatic pressure K_P of these fibres, which was measured by the fibre producers, was 138 rad/(MPam) and 98.3 rad/(MPam), respectively. Cross-sections of the SMPM-SH fibres were similar to that of the fibre shown in Fig. 2(b). The sensitivity K_F of these fibres, estimated from the size of their side holes, was 1.32 rad/N and 1.02 rad/N.

The measurements were carried out in a setup presented in Fig. 5. A linearly polarised HeNe laser was used as a light source. The light was coupled into the fibre under test using the microscope objective L_1 in such a way that both polarization modes were excited with equal amplitudes. The length of the fibre under test was approximately 5 m. A 100-mm long section of the fibre, located in the middle of the fibre was sandwiched between two flat aluminium

Table 4. Normalised sensitivity to transverse force K_{FN} of RH fibre for different fibre geometries. ◆– side hole would extend beyond cladding for this h and r_h.

Normalised sensitivity K_{FN} (rad/N)		Distance from core centre to hole perimeter h (μm)								
		5	10	15	20	25	30	35	40	45
Hole radius r_h (m]	5	0.753	0.808	0.892	0.939	0.963	0.975	0.980	0.980	0.980
	10	1.261	0.828	0.828	0.869	0.896	0.906	0.902	◆	◆
	15	2.076	1.087	0.880	0.832	0.806	◆	◆	◆	◆
	20	3.108	1.509	1.090	◆	◆	◆	◆	◆	◆

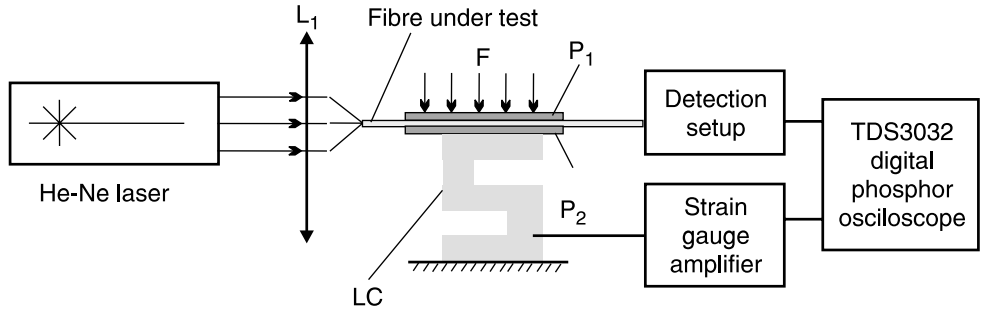

Fig. 5. System for measuring fibre sensitivity to the transverse force K_F.

plates P_1 and P_2. The bottom plate P_2 was fixed to the top of a load cell *LC* type S2 made by Hottinger Baldwin Messtechnik (Germany). Accuracy of load measurement in the setup being described is about 0.1%. The top plate, to which the force F_P was applied, rested entirely on the fibre. Detection setup employed in the experiment was a two-channel setup using a non-polarizing beamsplitter. The setup was described and analysed elsewhere [8]. Signal from the setup as well as the amplified signal from the load cell were recorded by a Tektronix TDS3032 Digital Phosphor Oscilloscope.

Both SMPM-SH fibres were more sensitive to the angular alignment of the axes of their elliptical core in the measurement setup than the standard SMPM fibre. Any misalignment between the direction in which the force was applied and the direction of the elliptic core's axis, resulted in fluctuations of the received signal level, presumably caused by coupling of polarization modes in the fibre under test.

Dependence of phase change $\Delta\varphi$ of polarization modes from applied force for all investigated fibres is shown in Fig. 6. Based on these results, sensitivity of the fibres to transverse force K_F was calculated. For the standard fibre K_F = 0.41 rad/N, whereas for BT fibres type 960613 XI and 960308 VI K_F equals 0.77 rad/N and 0.73 rad/N, respectively. The measured sensitivity K_F of the standard SMPM fibre is equal to that predicted from modelling [9]. Sensitivity of the SMPM-SH fibres is lower in both cases, by 42% for 960613 XI fibre, and by 28% for 960308 VI fibre.

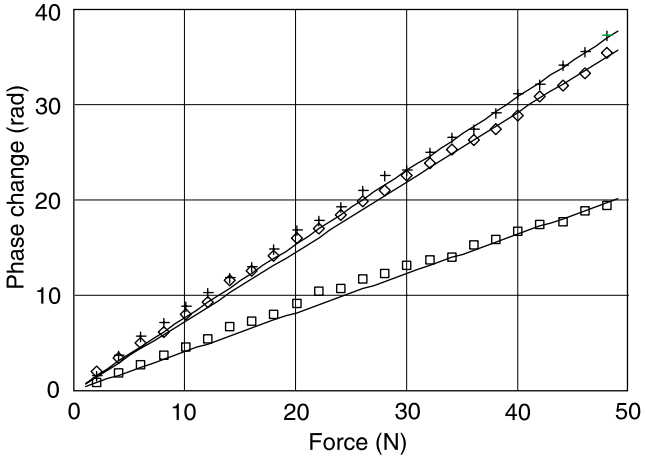

Fig. 6. Change of phase difference of polarization modes versus force for tested fibres. Measurement data points: □ – standard SMPM fibre, + – SMPM-SH fibre 960613 XI, ◊ – SMPM-SH fibre 960308 VI. Solid lines denote results of least-square fitting for respective measurement data sets.

The discrepancy between the calculated and measured values K_F is caused by lack of concentricity of the fibre in its coating, which was visible under microscope, and by misalignment between the direction in which the pressure was applied and the direction of the elliptic core's axis. This discrepancy can also be increased by simplifications made during modelling, such as assumption of isotropic properties of coating material.

5. Conclusions

Presented results of modelling and experiment show that selected types of SMPM-SH fibres have higher sensitivity to the transverse force K_F than that of a standard SMPM fibre. An increase of up to three times is possible according to finite element modelling. Experiment conducted with an SMPM-SH fibre which according to finite element modelling has sensitivity 136% higher than that of a standard fibre yielded an increase of 88%. The difference is attributed to the eccentric orientation of the fibres in the coating and to their inaccurate orientation in measurement setup. To address the problem of fibre alignment, a new, more accurate setup will be designed, which will allow the measurements to be performed with greater accuracy and repeatability.

It is important to note that certain SMPM-SH fibres (i.e., RH fibres) do not have higher sensitivity to the transverse force K_F than the standard SMPM fibre. Therefore, the merits of different types of SMPM-SH fibres have to be assessed on an individual basis.

More systematic research is needed in order to investigate fully the behaviour of SMPM-SH fibres subjected to transverse force. This research should encompass a broad range of fibre types with different side hole shapes and different coating types, including hermetic or hard coating. The main focus of this research should be dependence of the sensitivity K_F to transverse force from the shape of side holes. At the same time attention should be given to problems of temperature influence on sensi-

tivity, local sensitivity changes caused by fluctuations of fibre's dimensions arising in the drawing process as well as minimising the influence of angular misalignment on sensitivity.

Acknowledgements

Thanks are due to Dr Jan Wójcik from Univeristy of Maria Curie-Skłodowska (Lublin, Poland) for his kind provision of SMPM-SH fibre samples and fruitful discussions.

References

1. J. Wójcik, P. Mergo, W. Urbańczyk, and W.J. Bock, "Possibilities of application of the side-hole circular core fibre in monitoring of high pressures", *IEEE Instrumentation and Measurement Technology Conference*, Ottawa, Canada 19-21 May 1997, 975–978 (1997).
2. S. Timoshenko, J.N. Goodier, *Theory of Elasticity*, McGraw-Hill, New York, Toronto, London, 1951.
3. J.I. Sakai and T. Kimura, "Birefringence and polarization characteristics of single-mode optical fibres under elastic deformation", *IEEE J. Quantum Electronics* **QE17**, 1041–1051 (1981).
4. J.I. Sakai and T. Kimura, "Polarisation behaviour in multiply perturbed single-mode fibres", *IEEE J. Quantum Electronics* **QE18**, 59–65 (1982).
5. M. Tsubokawa, T. Higashi, and Y. Negishi, "Mode couplings due to external forces distributed along a polarization-maintaining fibre: an evaluation", *Appl. Optics* **27**, 166–173 (1988).
6. J. Wójcik, P. Kurzynowski, W.A. Woźniak, and M. Małuszek, "Characterization of side-hole fibres with elliptical core", *Proc. SPIE* **3320**, 191–197 (1998).
7. M. Barbachi and J.M. Caussignac, "Development of a single-mode optical fibre sensor for civil engineering applications", *Proc. SPIE* **2718**, 398–407 (1996).
8. P. Wierzba and B.B. Kosmowski, "Polarimetric sensors for weigh-in motion of road vehicles", *Opto-Electron. Rev.* **8**, 181–187 (2000).
9. P. Wierzba, "Modelling of polarimetric sensors for weigh-in motion of road vehicles", *PhD Thesis*, Gdansk University of Technology, Faculty of Electronics, Telecommunication and Informatics, 2001. (in Polish).
10. W.J. Bock, M.R.H. Voet, M. Beaulieu, T.R. Wolinski, and J. Chen, "Prototype fibre-optic pressure cell for stress monitoring", *IEEE Transactions on Instrumentation and Measurement* **41**, 1045–1049 (1992).
11. R.B. Dyott, *Elliptical Fibre Waveguides*, Artech House, Boston, London, 1995.

Forthcoming conferences

Readers are invited to send the Executive Editor details of conference to be announced

February 2004

2–6
2004 Australian Conference on Microscopy and Microanalysis 18, Geelong, Australia
Analytical tools, as well as crystallography and materials characterization, will be discussed.
Tel:+61 3 5227 8121
E-mail: luco@ideakin.edu.au
URL: www.deakin.edu.au/events/acmm18/

9–13
Interplay of Magnetism and Structure in Functional Materials, Benasque, Spain
Sessions on magnetoelastic materials, magnetocaloric effect, and colossal magnetoresistance.
Tel: +3493402 11 89
E-mail: lluis@ecm.ub.es
URL: www.ecm.ub.es/workshop2004/

11–12
Medical Device Technology 2004, Birmingham, UK
Conference includes plenary and interactive sessions on innovative materials, design and manufacturing, medical device and in vitro diagnostics regulation.
Tel: +44 (0)208 987 0900
E-mail: cmott@advanstar.com
URL: www.mdtevents.com

14–19
ISSCC 2004: IEEE International Solid-State Circuits Conference, San Francisco, CA, USA
Discussions will focus on memory, MEMS, signal processing, and wireless communication systems.
Tel: +1 2029738667
E-mail: ISSCC@courtesyassoc.com
URL: www.sscs.org

15–18
27th Annual Meeting of the Adhesion Society, Wilmington, NC, USA
Topics include smart adhesion, structural adhesives, surface chemistry, modification, and modeling
Tel: +1 540 231 7257
E-mail: adhesoc@vt.edu
URL: www.adhesionsociety.org

20
Characterization of Vacancy-Related Defects in Materials, London, UK
One-day conference organized by the Institute of Physics.
Contact: Dawn Stewart
Tel: +44 (0) 20 470 4800
E-mail: dawn.stewart@iop.org
URL: www.iop.org

22–27
29th Annual International Symposium on Microlithography, Santa Clara, CA, USA
Sessions cover emerging lithographic and resist technologies, metrology, and process control.
Tel: +1 3606763290
E-mail: spie@spie.org
URL: www.spie.org

22–27
Dynamics of Disordered Materials on the Nanometer Scale, Hanoi, Vietnam
Conference will review the dynamics of disordered systems including: embedded and freestanding nanoparticles; polymer-nanoparticle composites; and the bio-nano interface.
Tel:+1 7182603743
E-mail: info@eci.poly.edu
URL: www.engconfintl.org/4ah.html

25–29
Conference on Photo-responsive Materials, Kariega Game Reserve, South Africa
Focusing on Ill-nitrides, chalcopyrites, wide band gap materials, crystal growth, characterization, defect-related studies, and opto-electronic devices.
Tel: +27 41 504 2259
E-mail: ernest.vandyk@upe.ac.za
URL: www.upe.ac.za/kariegaconf

26
International Symposium on Advanced Materials for Fluid Machinery, London, UK
Event will review the availability of superior materials and successes in their use over the last ten years.
Contact: Madeline Willis
Tel: +44 (0)20 7973 1260
E-mail: M_Willis@imeche.org.uk
URL: www.imeche.org.uk

March 2004

1–4
ICMI 2004: 5th International Conference on Microelectronics and Interfaces, Santa Clara, CA, USA
Thin films, vacuum technology, nanodevice fabrication and processing, and new analytical and metrology techniques will be discussed.
Tel: +1 408 2463600
E-mail: della@avs.org
URL: www.avs.org

7–11
Nanotech 2004, Boston, MA, USA
Conference consists of four tracks on nano-, bio-, and microtechnology, as well as business and investment.
Tel: +1 925 901 4959
E-mail: wenning@nsti.org
URL: www.nanotech2004.com

7–11
PECS-V: International Symposium on Photonic and Electromagnetic Crystal Structures V, Kyoto, Japan
Sessions will focus on photonic crystal materials and structures; modeling; novel phenomena in photonic crystals; devices, and integration.
E-mail: pecs-v@qoe.kuee.kyoto-u.ac.jp
URL: www.kuee.kyoto-u.ac.jp/~lab05/pecs-v.html

7–12
PITTCON 2004, Chicago, IL, USA
Symposia on analytical techniques, characterization, spectroscopy, microfluidics, and nanotechnology.
Tel: +1 4128253220
E-mail: info@pittcon.org
URL: www.pittcon.org

14–18
SPIE 11th Annual International Symposium on Smart Structures and Materials, San Diego, CA, USA
Sessions on: electroactive polymer actuators and devices; active materials; applications; smart electronics; MEMS, BioMEMS, and nanotechnology.
Tel: +1 360/676-3290
E-mail: spie@spie.org
URL: www.spie.org

19–22
MAPEES '04: Novel Materials Processing by Advanced Electromagnetic Energy Sources, Osaka, Japan
Encompassing all aspects of novel materials processing by advanced electromagnetic energy sources.
E-mail: mapees@jwri.osaka-u.ac.jp
URL: www.jwri.osaka-u.ac.jp/-conf/mapees04/

